

Magnetoexcitons in transition-metal dichalcogenides monolayers, bilayers, and van der Waals heterostructures

Roman Ya. Kezerashvili^{1,2} and Anastasia Spiridonova^{1,2}

¹*The Graduate School and University Center, The City University of New York, New York, NY 10016, USA*

²*New York City College of Technology, The City University of New York, Brooklyn, NY 11201, USA*

(Dated: July 14, 2022)

We study direct and indirect magnetoexcitons in Rydberg states in monolayers and heterostructures of transition-metal dichalcogenides (TMDCs) in an external magnetic field, applied perpendicular to the monolayer or heterostructures. We calculate binding energies of magnetoexcitons for the Rydberg states $1s$, $2s$, $3s$, and $4s$ by numerical integration of the Schrödinger equation using the Rytova-Keldysh potential for direct magnetoexcitons and both the Rytova-Keldysh and Coulomb potentials for indirect magnetoexcitons. Latter allows understanding the role of screening in TMDCs heterostructures. We report the magnetic field energy contribution to the binding energies and diamagnetic coefficients (DMCs) for direct and indirect magnetoexcitons. The tunability of the energy contribution of direct and indirect magnetoexcitons by the magnetic field is demonstrated. It is shown that binding energies and DMCs of indirect magnetoexcitons can be manipulated by the number of hBN layers. Therefore, our study raises the possibility of controlling the binding energies of direct and indirect magnetoexcitons in TMDC monolayers, bilayers, and heterostructures using magnetic field and opens an additional degree of freedom to tailor the binding energies and DMCs for heterostructures by varying the number of hBN sheets between TMDC layers. The calculations of the binding energies and DMCs of indirect magnetoexcitons in TMDC heterostructures are novel and can be compared with the experimental results when they will be available.

I. INTRODUCTION

Transition-metal dichalcogenides (TMDCs) present a great interest for application in nano- and quantum devices at room temperature owing to Dirac cone [1–10], direct gap at nonequivalent points K/K' [11–13], and strong-spin orbit interaction that lifts degeneracy at valence and conduction bands [14–16]. In design of electronic devices, TMDCs monolayers, TMDC/TMDC, and TMDC/insulator/TMDC heterostructures can be used. Moreover, TMDCs present a great interest for fundamental research. TMDCs heterostructure can support high-temperature quantum Bose gases of indirect excitons [17–20], superfluidity of electron-hole [21, 22] and dipolar excitons [23], and superconductivity [24].

TMDCs are semiconductors that have a chemical formula MX_2 where M is a transition metal atom (Mo or W) and X is a chalcogen atom (S, Se, or Te). The comprehensive review of excitonic complexes in TMDCs monolayers is given in Refs. [14, 25, 26]. Excitons in monolayers have a direct energy gap. However, TMDCs heterostructures made of monolayers have indirect gaps. There are two possible arrangements of double-layer heterostructures: bilayer TMDC-TMDC [19, 20, 27–37] and TMDC-insulator-TMDC [17, 35, 38]. For both arrangements, there are two types of heterostructures. Type-I heterostructure is a heterostructure formed by the same type of TMDC monolayers [19, 29, 35, 39], and type-II heterostructure is formed by monolayers of different TMDC monolayers [20, 23, 27, 28, 30–37, 40]. Both type-I and II heterostructures have indirect band gap [39, 41–43]. However, stacking order [39, 44] or application of strain [43] can be used to induce indirect gap into direct gap. In addition, the application of perpendicular electric field controlled by voltage modifies the band structure so it is advantageous for electrons and holes to reside in different TMDC layers [17, 19, 45] and makes indirect excitons more preferable than direct excitons. However, the application of the electric field can lead to dissociation of indirect excitons [46]. Nevertheless, the extended lifetime of indirect excitons [28, 29, 34, 47] compared to direct excitons presents great interest for the design of electronic devices.

The history of studying excitons in semiconductors in the magnetic field extends back for 60 years. Starting from Elliot and Loudon [48] and Hasegawa and Howard [49], who developed the theory of the Mott exciton in the strong magnetic field followed by authors of Refs. [50–52], who studied the physics of Mott magnetoexcitons. For direct magnetoexcitons in TMDCs, the binding energies of Rydberg states of direct excitons are reported in Refs. [53–59], the Zeeman (ZM) shift has been considered in Refs. [54, 56–58, 60–69], and the diamagnetic (DM) shift was addressed in Refs. [54–58, 60, 63, 64, 66, 68, 70–74]. For indirect excitons in double-layer heterostructures Rydberg states binding energies are reported in [20, 28–30, 34, 35, 39, 40, 46, 75–77], and Zeeman shift is addressed in Refs. [33, 78–82].

Historically, the electromagnetic interaction between electron and hole was described by Coulomb potential (V_C) for both direct and indirect excitons [48, 50–52, 83–88]. However, as has been shown, the Rytova-Keldysh (RK) potential (V_{RK}) [89, 90] is the appropriate potential to describe the interaction of electron and hole in two-dimensional (2D) configuration space since the RK potential takes into account the effects of the dielectric environment and the 2D confinement. As a result, currently, both the RK [26, 54, 55, 57–59, 65, 68, 72, 91–94] and Coulomb potential are

used to describe the direct exciton. For indirect excitons, the Coulomb potential is used. However, in a few cases, the RK potential is used as well. We do the same thing: we use both the RK and Coulomb potentials for indirect exciton to investigate the importance of using the accurate potential that describes an interaction between hole and electron.

In this paper, we study the effects of the external magnetic field on the binding energies of $1s$, $2s$, $3s$, and $4s$ Rydberg states of direct and indirect magnetoexcitons in TMDCs. A and B direct magnetoexcitons are considered in freestanding (FS) and encapsulated by the hexagonal boron nitride (hBN) MX_2 monolayers, and A and B indirect magnetoexcitons are considered in bilayer MX_2 - MX_2 and MX_2 -hBN- MX_2 type-I heterostructures. In our study to find eigenfunctions and eigenenergies for indirect magnetoexcitons, a two-particle Schrödinger equation is solved using the Rytova-Keldysh [89, 90] and Coulomb potentials to calculate binding energies and diamagnetic coefficients. We demonstrate strong sensitivity of the energy contributions from the external magnetic field on the type of the potential. The first time diamagnetic coefficients (DMCs) for bilayer MX_2 - MX_2 and MX_2 -hBN- MX_2 heterostructures are calculated and reported. Our study raises the possibility to control the binding energies of direct and indirect magnetoexcitons in monolayer MX_2 , bilayer MX_2 - MX_2 , and MX_2 -hBN- MX_2 heterostructures using a magnetic field and opens an additional degree of freedom to tailor the binding energies and DMCs for heterostructures by varying the number of hBN sheets between TMDC layers.

The article is structured as follows. In Sec. II we introduce the theoretical formalism for the description of Mott-Wannier magnetoexcitons in freestanding and encapsulated MX_2 monolayers, and in TMDC heterostructures and discuss electrostatic interactions that form direct and indirect magnetoexcitons. In Sec. III we focus on the analysis and discussion of the results. In particular, contributions from the external magnetic field to binding energies of magnetoexcitons in MX_2 monolayers, MX_2 - MX_2 bilayers, and MX_2 -hBN- MX_2 heterostructures are presented and discussed in Subsecs. III A and III B, respectively. Subsec. III C is devoted to the calculations of diamagnetic coefficients for direct and indirect magnetoexcitons. Finally, Sec. IV concludes upon the results.

II. THEORETICAL FORMALISM

In this section, we provide the theoretical formalism for describing the Mott-Wannier magnetoexciton in 2D materials and present the energy contribution from the external magnetic field to the Rydberg states binding energy of magnetoexcitons. Here, we present electrostatic interactions that due to a non-local dielectric screening of an electron-hole interaction strongly modify the electrostatic Coulomb potential and form direct magnetoexcitons in TMDC monolayers and indirect magnetoexcitons in MX_2 - MX_2 bilayers and MX_2 -hBN- MX_2 van der Waals heterostructure, where N layers of hBN monolayers separate two TMDC monolayer

A. Mott-Wannier magnetoexciton in 2D materials

Let us introduce the equation for the description of Mott-Wannier excitons in the external magnetic field. We employ an effective mass model for two charged point-like particles in two dimensions. In general, electrostatically-bound electrons and holes in the external magnetic field form magnetoexcitons. To find the eigenfunctions and eigenenergies of a 2D magnetoexciton in TMDCs monolayer, bilayer MX_2 - MX_2 , and MX_2 -hBN- MX_2 heterostructure in the external magnetic field, we write the Schrödinger equation for an interacting electron and hole [85] ($\hbar = c = 1$):

$$\left[\frac{1}{2m_e} \left(-i\nabla_e + e\mathbf{A}(\mathbf{r}_e) \right)^2 + \frac{1}{2m_h} \left(-i\nabla_h - e\mathbf{A}(\mathbf{r}_h) \right)^2 + V(r_e, r_h) \right] \psi(\mathbf{r}_e, \mathbf{r}_h) = E\psi(\mathbf{r}_e, \mathbf{r}_h), \quad (1)$$

where e is the charge of the electron, the indices e and h are referring to the electron and hole, respectively, \mathbf{r}_e and \mathbf{r}_h are 2D coordinates and m_e and m_h are the masses of charged particles, $\mathbf{A}(\mathbf{r}_{e/h}) = \mathbf{B} \times \mathbf{r}_{e/h}/2$ is a gauge vector potential, and $V(r_e, r_h)$ is the potential of interaction between the electron and hole confined in 2D space. In three-dimensional (3D) homogeneous dielectric environments, the electron-hole interaction is described by the Coulomb potential. However, in 2D monolayer this interaction has to be modified, because of the reduced dimensionality and screening effects. The original derivation of two charged particles interaction in 2D space was given by Rytova [89] and a decade later was independently obtained by Keldysh [90]. The potential is called the Rytova-Keldysh (RK) potential. For almost a decade, the RK potential has been used to describe electrostatic interaction between charge carriers of few-body complexes in transition-metal dehydrogenizes, phosphorene, and Xenon monolayers [26] and references herein.

Following Refs. [48, 50–52, 85, 88], in Eq. (1) we introduce the coordinate of the center-of-mass $\mathbf{R} = \frac{m_e\mathbf{r}_e - m_h\mathbf{r}_h}{M}$ and the relative motion coordinate $\mathbf{r} = \mathbf{r}_e - \mathbf{r}_h$, where the total mass of the system is $M = m_e + m_h$, and consider the magnetic field pointing in z -direction that is perpendicular to the monolayer where the exciton is located, $\mathbf{B} = \mathbf{B}(0, 0, B)$. After performing the standard procedure for the coordinate transformation to the center-of-mass, Eq. (1) becomes:

$$\left[-\frac{1}{2M} \frac{\partial^2}{\partial \mathbf{R}^2} - \frac{1}{2\mu} \frac{\partial^2}{\partial \mathbf{r}^2} + \frac{e^2}{8\mu} (\mathbf{B} \times \mathbf{R})^2 + \frac{e^2\mu^2}{8} \left(\frac{1}{m_e^3} + \frac{1}{m_h^3} \right) (\mathbf{B} \times \mathbf{r})^2 - \frac{ie}{2M} (\mathbf{B} \times \mathbf{r}) \cdot \frac{\partial}{\partial \mathbf{R}} - \frac{ie}{2\mu} (\mathbf{B} \times \mathbf{R}) \cdot \frac{\partial}{\partial \mathbf{r}} - \frac{ie\gamma}{2\mu} (\mathbf{B} \times \mathbf{r}) \cdot \frac{\partial}{\partial \mathbf{r}} + \frac{e^2\gamma}{4\mu} (\mathbf{B} \times \mathbf{R}) \cdot (\mathbf{B} \times \mathbf{r}) + V(\mathbf{r}) \right] \psi(\mathbf{R}, \mathbf{r}) = E\psi(\mathbf{R}, \mathbf{r}), \quad (2)$$

where $\gamma = \frac{m_h - m_e}{m_h + m_e}$ and $\mu = \frac{m_e m_h}{m_e + m_h}$ is the reduced mass. Equation (2) is written for the case when masses of the electron and hole are different: $m_h \neq m_e$, which is the case in TMDCs. The term $(\mathbf{B} \times \mathbf{r}) \cdot \frac{\partial}{\partial \mathbf{r}} = \mathbf{B} \cdot \mathbf{L} = 0$ since we consider Rydberg states: $1s, 2s, 3s$, and $4s$, for which $l = 0, m_l = 0$.

Following Refs. [51, 85, 88], we introduce an operator $\hat{\mathbf{P}}$:

$$\hat{\mathbf{P}} = -i\nabla_{\mathbf{R}} - \frac{e}{2}(\mathbf{B} \times \mathbf{r}). \quad (3)$$

It is easy to check that $\hat{\mathbf{P}}$ commutes with the Hamiltonian in Eq. (1), therefore, it has the same eigenfunction as Eq. (1). Thus, one can write the wave function for the exciton in the magnetic field as [51, 88]:

$$\psi(\mathbf{R}, \mathbf{r}) = e^{[i\mathbf{R} \cdot (\mathbf{P} + \frac{e}{2}\mathbf{B} \times \mathbf{r})]} e^{\frac{1}{2}i\gamma\mathbf{r} \cdot \mathbf{P}} \Phi(\mathbf{r} - \tilde{\rho}_0), \quad (4)$$

where the notation $\tilde{\rho}_0 = \frac{1}{eB^2}(\mathbf{B} \times \mathbf{P})$ is introduced. After substituting the wave function $\psi(\mathbf{R}, \mathbf{r})$ in Eq. (2), the Schrödinger equation for the relative motion of the electron and hole reads:

$$\left[\frac{\mathbf{P}^2}{4\mu} + \frac{e}{4\mu} \mathbf{P} \cdot (\mathbf{B} \times \mathbf{r}) - \frac{1}{2\mu} \frac{\partial^2}{\partial r^2} + \frac{e^2}{8\mu} (\mathbf{B} \times \mathbf{r})^2 - \frac{ie\gamma}{2\mu} (\mathbf{B} \times \mathbf{r}) \cdot \frac{\partial}{\partial \mathbf{r}} - \frac{i\gamma}{2\mu} \mathbf{P} \frac{\partial}{\partial \mathbf{r}} + V(r) \right] \Phi = E\Phi. \quad (5)$$

Finally, the equation for a 2D electron-hole pair with zero center-of-mass momentum reads [86, 88]:

$$\left[-\frac{1}{2\mu} \frac{\partial^2}{\partial r^2} + \frac{e^2}{8\mu} (\mathbf{B} \times \mathbf{r})^2 + V(r) \right] \Phi(r) = E\Phi(r). \quad (6)$$

Equation (6) describes the Mott–Wannier magnetoexciton in Rydberg optical states in 2D materials. This equation has a long history of the solution in the case of the electron-hole Coulomb interaction [48, 50–52, 83–88]. However, we solve Eq. (6) using V_{RK} for direct magnetoexcitons. For indirect magnetoexcitons, both V_{RK} and V_C potentials are used to investigate the importance of using correct potential describing electron-hole interactions. Note that Eq. (6) does not explicitly contain any spin- or valley-dependent Zeeman terms. Therefore, the eigenenergies correspond to the average transition energy of each exciton state between points K and K' [56].

By calculating the magnetoexciton energy of Rydberg states at different values of the magnetic field, we can find the energy contribution from the magnetic field to the binding energy of a magnetoexciton in the following way:

$$\Delta E = E_0 - E(B). \quad (7)$$

In Eq. (7) E_0 is the exciton energy when the magnetic field is absent, while $E(B)$ is the magnetoexciton energy at some value of the magnetic field.

In literature, the Zeeman and diamagnetic shifts of excitons in TMDCs monolayers are treated in the same way as ZM and DM shifts of excitons in quantum wells and quantum dots [95–103]. The first step is to write a magnetoexciton energy using Taylor series [97]:

$$E(B) = E_0 + \gamma_1 B + \gamma_2 B^2 + \dots \quad (8)$$

In Eq. (8) the second and third terms are the ZM and DM shifts, respectively. When the magnetic field's energy contribution is small compared to the binding energy in the absence of the magnetic field, we can use the first three terms of Taylor series to describe the magnetoexciton binding energy [68, 97, 99, 101]. In other words, the following condition $E_0 > |E(B) - E_0|$ is met. However, when $E_0 \sim |E(B) - E_0|$, higher-order terms in Eq. (8) need to be considered.

As stated before, the treatment of the ZM and DM shifts of magnetoexcitons in TMDCs monolayers follows the same procedure applied for quantum dots and quantum wells. The second step in describing ZM and DM shifts is to define them by connecting shifts to terms of Taylor series. The Zeeman shift is defined as $\gamma_1 B = -\mu_B g B$ [60, 63, 65, 67, 68, 99, 101, 102], where g is the g factor and μ_B is Bohr magneton. Experimentally, the ZM shift is defined as energy difference between K/K' points i.e. $-\mu_B g B = E(K) - E(K')$ [54, 56–58, 64, 65, 67, 68, 100, 101]. The diamagnetic shift is defined as $\gamma_2 B^2 = \frac{e^2}{8\mu} \langle r^2 \rangle B^2$ [54, 56–58, 68, 95–103], where $\langle r^2 \rangle$ is the expectation value of r^2 over the exciton envelope wave function. In our work, we follow notation used for magnetoexciton diamagnetic coefficient in TMDCs monolayers i.e. $\gamma_2 = \sigma$ [54, 56–58, 63, 67]. According to Refs. [54, 56–58, 67, 95–103] the DMC for a carrier in a semiconductor is defined as $\sigma = \frac{e^2}{8\mu} \langle r^2 \rangle$. Therefore, by calculating DMCs, exciton radius, reduced mass, and dielectric properties of a material can be obtained [54, 56–58, 97]. Experimentally, the DM shift is defined as $\sigma B^2 = \frac{E(K) + E(K')}{2}$ [57, 60, 68, 99, 101, 103].

B. Magnetoexcitons in TMDCs monolayer

A non-local dielectric screening of an electron-hole interaction strongly modifies the electrostatic Coulomb potential. It leads to a non-hydrogenic Rydberg series of exciting magnetoexciton states. The Rytova-Keldysh potential has become a prevalent description of the electrostatic interaction of charge carriers in 2D systems. The RK potential is central potential, and the interaction between the electron and hole for direct excitons in an encapsulated TMDC monolayer has the form [89, 90]:

$$V_{RK}(r) = -\frac{\pi k e^2}{2\kappa\rho_0} \left[H_0\left(\frac{r}{\rho_0}\right) - Y_0\left(\frac{r}{\rho_0}\right) \right], \quad (9)$$

where $r \equiv r_{eh} = r_e - r_h$ is the relative coordinate between the electron and hole. In Eq. (9), $\kappa = (\epsilon_1 + \epsilon_2)/2$ describes the surrounding dielectric environment, ϵ_1 and ϵ_2 are the dielectric constants below and above the monolayer, H_0 and Y_0 are the Struve and Bessel functions of the second kind, respectively, and $\rho_0 = 2\pi\chi_{2D}/\kappa$ [104] is the screening length, where χ_{2D} is the 2D polarizability of the monolayer, which is given by $\chi_{2D} = h\epsilon/4\pi$ [90], where ϵ is the bulk dielectric constant of the exciton/hole containing monolayer and h is the thickness of a TMDC monolayer. At $r < \rho_0$ the RK potential has logarithmical dependence and diverges logarithmically at the origin. At long-range distances, $r > \rho_0$, it retains the Coulomb potential behavior. Using the RK potential for description of excitons in 2D monolayer, one finds a strong dependence of the binding energy on whether the monolayer is suspended in air (Fig. 1a), encapsulated by hBN (Fig. 1b), or in heterostructures (Figs. 1c and 1d). It is worth mentioning that the RK potential is obtained for a monolayer. However, a TMDC monolayer consists of three atomic layers: chalcogen-metal-chalcogen sheets. To address this problem, a new potential is derived in Ref. [105] which considers the three atomic sheets that compose a monolayer of TMDC and can explain the nonhydrogenic Rydberg series of excitons in TMDC monolayer. The Rytova-Keldysh potential can be recovered when considering the strict 2D limit, and in our study, we are using the RK potential.

C. Indirect magnetoexcitons in TMDCs heterostructures

Van der Waals-like forces can hold together layered TMDC materials. When two TMDC monolayers are brought together, the conduction band minimum, and the valence band maximum reside in two different layers. Electrons and holes in such a structure prefer to reside in separate layers [46]. Let us now consider the formation of indirect magnetoexcitons formed by electrons and holes in type-I heterostructure molded by the same type of TMDC monolayers: a bilayer $\text{MX}_2\text{-MX}_2$ heterostructure, shown in Fig. 1c and van der Waals $\text{MX}_2\text{-hBN-MX}_2$ heterostructure, presented in Fig. 1d. Such magnetoexcitons have a longer lifetime than the direct excitons due to longer recombination time. In such structures, the electron and hole move in the planes of different layers, form an indirect exciton, and have restricted motion between the layers due to the dielectric barrier. The latter is a two-body problem in the restricted 3D space, and the electrostatic electron-hole interaction $V(r)$ could form a bound state, i.e., the indirect magnetoexciton. Therefore, to determine the binding energy of the magnetoexciton one must solve a two-body problem in restricted 3D space because the motion in z -direction is restricted. The relative separation r between the electron and hole can be written in cylindrical

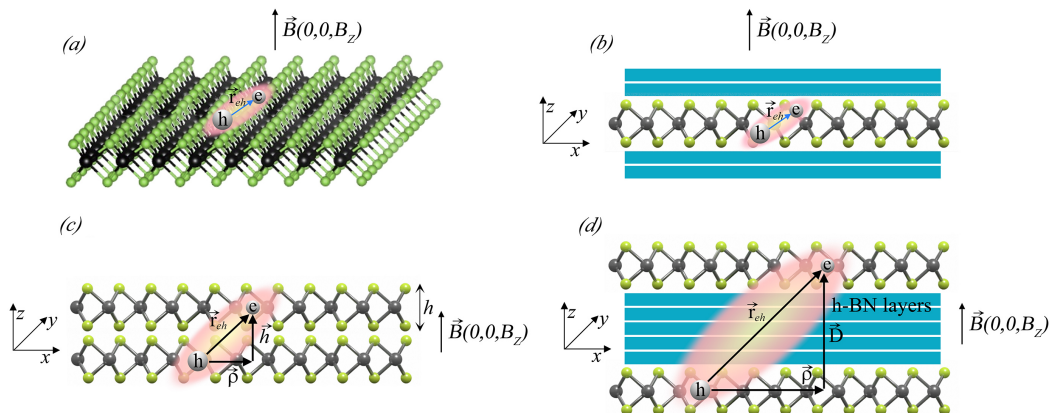


FIG. 1. (Color online) Schematic illustration of magnetoexcitons in TMDC monolayers and heterostructures. (a) A direct magnetoexciton in a freestanding TMDC monolayer. (b) A direct magnetoexciton in an encapsulated TMDC monolayer. (c) An indirect magnetoexciton in a freestanding bilayer $\text{MX}_2\text{-MX}_2$ heterostructure. (d) An indirect magnetoexciton in $\text{MX}_2\text{-hBN-MX}_2$ van der Waals heterostructure.

coordinates as $\mathbf{r} = \rho\hat{\boldsymbol{\rho}} + D\hat{\mathbf{z}}$, where $\hat{\boldsymbol{\rho}}$ and $\hat{\mathbf{z}}$ are unit vectors. Writing r in cylindrical coordinates allows us to treat the case of direct excitons in a TMDC monolayer and spatially indirect excitons in bilayer $\text{MX}_2\text{-MX}_2$ and $\text{MX}_2\text{-hBN-MX}_2$ heterostructures on equal footing. If we set $D = 0$ in the latter expression, it becomes a purely 2D equation, with ρ representing the separation between the electron and hole sharing the same plane. For spatially indirect excitons, the relative distance between the electron and hole is $r = \sqrt{\rho^2 + D^2}$, where D is the distance between the middle of two TMDC layers assuming that the electron and hole reside in the middle of their respective sheets [46].

Thus, for the description of indirect Mott–Wannier magnetoexcitons one can use Eq. (6) with interactions

$$V_{RK}(\sqrt{\rho^2 + D^2}) = -\frac{\pi k e^2}{2\kappa\rho_0} \left[H_0 \left(\frac{\sqrt{\rho^2 + D^2}}{\rho_0} \right) - Y_0 \left(\frac{\sqrt{\rho^2 + D^2}}{\rho_0} \right) \right] \quad (10)$$

for the RK potential, and

$$V_C(\sqrt{\rho^2 + D^2}) = -\frac{k e^2}{\kappa(\sqrt{\rho^2 + D^2})} \quad (11)$$

for the Coulomb potential. Equations (10) and (11) describe the interaction between the electron located in one and hole in the other parallel TMDC monolayers. Therefore, one can obtain the eigenfunctions and eigenenergies of magnetoexcitons by solving Eq. (6) using the potential (9) for direct magnetoexcitons, or using either potential (10) or (11) for indirect magnetoexcitons. For indirect magnetoexcitons, we perform calculations using both the RK and Coulomb potentials. This allows a better understanding of the importance of the screening effect in $\text{MX}_2\text{-MX}_2$ and $\text{MX}_2\text{-hBN-MX}_2$ heterostructures.

It is worth mentioning that the RK potential was originally formulated as an explicitly 2D description of the Coulomb interaction. Nevertheless, there have been recent attempts to apply the RK potential to indirect excitons in van der Waals heterostructures of 2D materials such as the TMDCs, phosphorene, and Xenon [17, 18, 23, 77, 106–108]. The logic behind considering the RK potential for indirect excitons follows from two considerations: i. the dielectric environment is still inhomogeneous, just as in the case of the direct exciton – when the interlayer separation D is smaller than, or comparable to, the RK potential screening length ρ_0 and the excitonic gyration radius $\sqrt{\langle r^2 \rangle}$, the electron-hole interaction potential must account for both the TMDC monolayers and the interlayer dielectric, and ii. as the interlayer separation D becomes larger than ρ_0 , the total separation between the electron and hole, $r = \sqrt{\rho^2 + D^2}$, becomes much larger than ρ_0 , and, therefore, the RK potential converges towards the Coulomb potential. Let us emphasize that we are not claiming definitively that the RK potential provides the most accurate description of the spatially indirect exciton, hence, we present the extensive comparison with the corresponding results calculated using the Coulomb potential.

Above, we consider ideal cases when encapsulated TMDC monolayer, bilayer $\text{MX}_2\text{-MX}_2$, and $\text{MX}_2\text{-hBN-MX}_2$ heterostructures are fabricated so that each layered material is stacked without any vacuum or air interlayer gap. In reality, between the layers always exists non-vanishing interlayer gap. In each layer the field lines of the Coulomb interaction are screened by the adjacent material, which reduces the single-particle band gap as well as exciton binding energies [109]. In Ref. [109] the authors demonstrate and give a quantitative understanding that the binding energy of excitons and electronic and optical properties are sensitive to the interlayer distances on the atomic scale.

Throughout this paper, we consider the separation between the electron and hole residing in two TMDC monolayers of the $\text{MX}_2\text{-hBN-MX}_2$ van der Waals heterostructures in steps of calibrated thickness, $l_{\text{hBN}} = 0.333$ nm, corresponding to the thickness of one hBN monolayer: $D = h + Nl_{\text{hBN}}$, where h is the TMDC monolayer thickness and N is the number of hBN monolayers. For a bilayer $\text{MX}_2\text{-MX}_2$ heterostructure $N = 0$ and following Ref. [46] the electron and hole reside in the middle of their respective sheets and $r = \sqrt{\rho^2 + h^2}$.

III. RESULTS OF CALCULATIONS AND DISCUSSION

We report the energy contribution from the external magnetic field to the binding energies of A and B magnetoexcitons in Rydberg optical states $1s$, $2s$, $3s$, and $4s$, in freestanding (Figs. 1a) and encapsulated (Figs. 1b) WSe_2 , WS_2 , MoSe_2 , and MoS_2 monolayers, bilayer $\text{MX}_2\text{-MX}_2$ (Fig. 1c), and $\text{MX}_2\text{-hBN-MX}_2$ heterostructures (Fig. 1d). The diamagnetic coefficients for the bilayer $\text{MX}_2\text{-MX}_2$ and $\text{MX}_2\text{-hBN-MX}_2$ heterostructures are reported the first time. We are considering the further knob to tailor the binding energies and diamagnetic coefficients for the $\text{MX}_2\text{-hBN-MX}_2$ heterostructures by varying the number of hBN sheets between TMDC layers and present corresponding calculations. In our calculations, we vary the magnetic field in increment of 1 T in the range from 0 T to 30 T and use input parameters given in Table I. In Table I, the values of $E_{A_{\text{high}}}$ and $E_{A_{\text{low}}}$ correspond to the parameters found in the literature, which minimizes and maximizes the A exciton binding energy, respectively. It is highly likely that each parameter's true value for a given material falls somewhere within the range given. Therefore, the true magnitude of the calculated quantities for A excitons studied in this paper lies somewhere between the calculated values. Values of E_B correspond to parameters given in the literature for B excitons.

TABLE I. Parameters for the A and B excitons. For the A exciton for each material two values of μ and χ_{2D} are given. The average dielectric constant, $\kappa = \frac{\epsilon_1 + \epsilon_2}{2} = 4.89$, is taken from Ref. [17]. κ is the same for all materials. μ is in units of electron mass, m_0 . The 2D polarizability χ_{2D} and TMDC monolayer thickness h are given in Å.

		μ (m_0)	χ_{2D} (Å)	ρ_0 (Å)	h (Å)			μ (m_0)	χ_{2D} (Å)	ρ_0 (Å)	h (Å)
WSe ₂	$E_{A_{\text{high}}}$	0.27 [110]	7.18 [104]	9.226	6.575 [53]	MoSe ₂	$E_{A_{\text{high}}}$	0.31 [110]	8.23 [104]	10.575	6.527 [53]
	$E_{A_{\text{low}}}$	0.15 [111]	7.571 [53]	9.728			$E_{A_{\text{low}}}$	0.27 [104]	8.461 [53]	10.872	
	E_B	0.16 [53]	7.18 [104]	9.226			E_B	0.29 [53]	8.23 [104]	10.575	
WS ₂	$E_{A_{\text{high}}}$	0.23 [110]	6.03 [104]	7.748	6.219 [53]	MoS ₂	$E_{A_{\text{high}}}$	0.28 [110]	6.60 [104]	8.480	6.18 [53]
	$E_{A_{\text{low}}}$	0.15 [111]	6.393 [53]	8.214			$E_{A_{\text{low}}}$	0.16 [92]	7.112 [53]	9.138	
	E_B	0.15 [53]	6.03 [104]	7.748			E_B	0.24 [53]	6.60 [104]	8.480	

A. Contribution from the external magnetic field to binding energies of magnetoexcitons in a monolayer

The results of the energy contribution from the magnetic field to the binding energy for direct A and B of Rydberg states magnetoexcitons in freestanding and encapsulated TMDC monolayers are reported in Fig. 2. The comparative analysis of the results presented in Fig. 2 shows the following: i. the energy contribution from the magnetic field to the binding energy of the direct magnitoexcitons in FS monolayers of TMDC materials is always less than in encapsulated monolayers, and the difference increases with the increase of the magnetic field; ii. the direct magnetoexcitons in FS monolayers are bound in $1s$, $2s$, $3s$, and $4s$ states within all considered range of the magnetic field, while magnetoexcitons in encapsulated monolayers dissociated in the states $3s$ and $4s$ when the magnetic field is greater than some particular values. These conclusions are related to the direct A_{low} magnetoexcitons. Interestingly enough that these conclusions stay the same for direct A_{high} and B magnetoexcitons. However, the ΔE is systematically smaller for the A_{high} , while ΔE for B magnetoexcitons are lying between ΔE for the A_{low} and A_{high} magnetoexcitons.

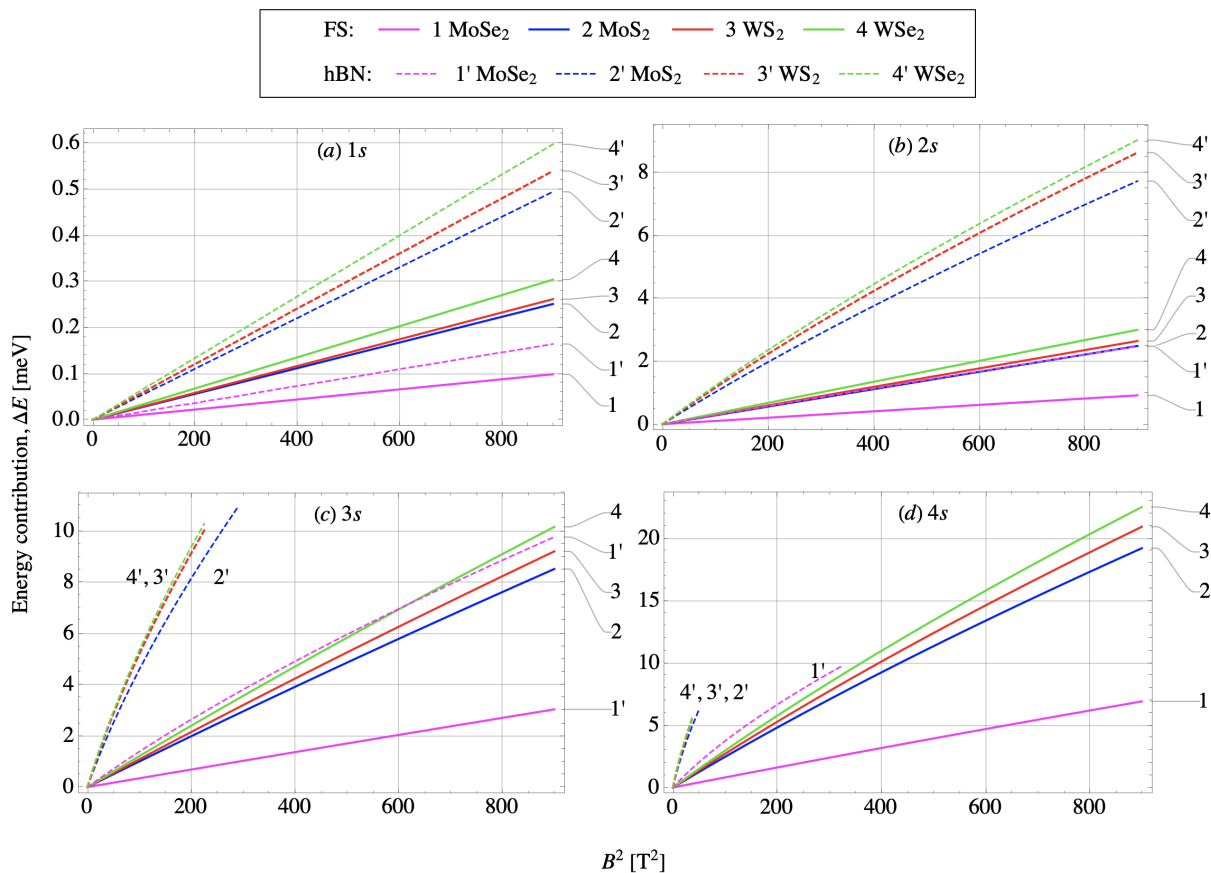


FIG. 2. Energy contribution from the magnetic field to the binding energies of Rydberg states $1s$ (a), $2s$ (b), $3s$ (c), and $4s$ (d) for direct A_{low} magnetoexcitons in FS and encapsulated by hBN MX₂ monolayers. The solid and dashed curves present results of calculations for freestanding and encapsulated TMDC monolayers, respectively.

Analysis of the results shows that the energy contribution from the external magnetic field to the magnetoexciton binding energy depends on material parameters. In fact, the binding energy of magnetoexcitons is a function of the reduced mass μ and polarizability χ_{2D} : the binding energy of a magnetoexciton is bigger for the smaller μ and larger χ_{2D} . This pattern qualitatively coincides with previously reported calculations for magnetoexcitons in WSe₂ and MoSe₂ monolayers [74]. It is worth noting that for MoS₂ the energy contribution from the magnetic field for the state 1s is more than one order of magnitude smaller than for the states 2s, 3s and 4s. Another distinct feature is that magnetoexcitons are ionized in states 3s and 4s at some of the magnetic field values while staying bound in states 1s and 2s at higher magnetic field values.

B. Contribution from the external magnetic field to binding energies of magnetoexcitons in bilayer MX₂-MX₂ and MX₂-hBN-MX₂ heterostructures

As the first step, we compare the contributions to binding energies of indirect magnetoexcitons due to the external magnetic field calculated using the RK and Coulomb potentials. In Fig. 3 are shown the energy contributions from the magnetic field to the binding energies of indirect magnetoexcitons in FS bilayer MoS₂-MoS₂ for Rydberg states 1s (3a), 2s (3b), 3s (3c), and 4s (3d). The binding energies are calculated using V_{RK} and V_C potentials. Data are plotted for A_{high} , A_{low} , and B magnetoexcitons. The comparison shows that i. $\Delta E_{RK} > \Delta E_C$ and the difference increases with the magnetic field increase; ii. results obtained with both potentials satisfy the following inequality: $\Delta E_{A_{\text{high}}} < \Delta E_B < \Delta E_{A_{\text{low}}}$. Most importantly, it is worth to mention that the contribution from the magnetic field is systematically bigger for the FS bilayer MoS₂-MoS₂ than for the FS MoS₂ monolayer for all states when calculations are performed with V_{RK} . In other words, $\Delta E_{A_{\text{low}}}$ for indirect magnetoexcitons in FS MoS₂-MoS₂ bilayer is greater than $\Delta E_{A_{\text{low}}}$ for direct magnetoexcitons in FS MoS₂ monolayer. Similar patterns are observed for other FS bilayers constituent from MoSe₂, WS₂ and WSe₂ monolayers, respectively.

Now let us consider indirect magnetoexcitons in MoS₂-hBN-MoS₂ heterostructure. In Fig. 4 are presented the results of calculations for the dependence of the ratio $\Delta E_{RK}/\Delta E_C$ on the magnetic field and number of the hBN

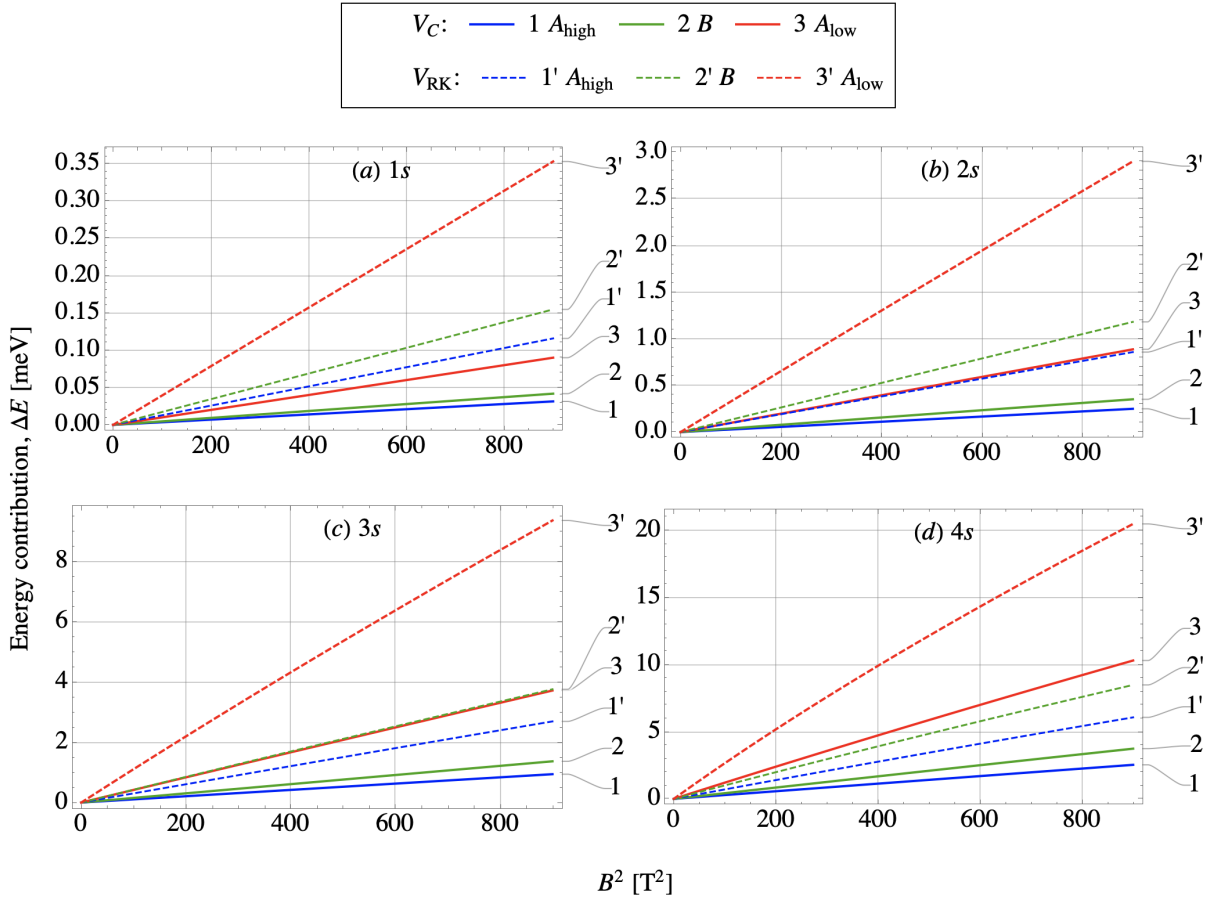


FIG. 3. Energy contribution from the magnetic field to the binding energies of Rydberg states 1s (a), 2s (b), 3s (c), and 4s (d) for indirect magnetoexcitons in FS MoS₂-MoS₂ bilayer. The binding energy is calculated with V_{RK} (dashed lines) and V_C (solid lines) potentials. Data are plotted for A_{high} , A_{low} , and B magnetoexcitons.

layers separating two parallel TMDC layers. Calculations are performed for A magnetoexcitons. The ratio weakly depends on the magnetic field and converges towards 1 when the number of hBN layers increases. The RK potential always gives the larger contribution than the Coulomb potential. However, when the number of hBN layers is more than three, the difference becomes very small. Such a result is understandable because the potential $V_{RK}(\sqrt{\rho^2 + D^2})$ converges to $V_C(\sqrt{\rho^2 + D^2})$ when D increases.

The dependencies of the energy contribution to the binding energy of magnetoexcitons Rydberg states for indirect magnetoexcitons on the magnetic field and number of hBN layers for MoS₂-hBN-MoS₂ heterostructure are reported in Fig. 5. For $1s$ and $2s$ states the energy contribution increases with the increase of the external magnetic field and number of the hBN layers. Indirect magnetoexcitons ionize in state $3s$, when $B > 11 - 15$ T, and in $4s$ state, when $B > 5$ T. In Fig. 5a, it is shown the energy contribution for the B exciton always falls between $\Delta E_{A_{\text{high}}}$ and $\Delta E_{A_{\text{low}}}$: $\Delta E_{A_{\text{high}}} < \Delta E_B < \Delta E_{A_{\text{low}}}$. The same holds for the states $2s$, $3s$ and $4s$, but not shown in Figs. 5b, 5c and 5d. It is worth mentioning that Fig. 5. shows a representative case for indirect magnetoexcitons in MoS₂-hBN-MoS₂ heterostructure. The same kind patterns and quantitative dependencies we obtained for the MoSe₂-hBN-MoSe₂ heterostructures. The differences occur only in the energy contribution magnitudes, which varies within up to 40% for MoSe₂-hBN-MoSe₂ for the maximum value and indirect magnetoexcitons do not ionize in the $3s$ state and are ionized at larger values of the magnetic field in $4s$ state. In Fig. 6 are presented results for the tangerine-based WSe₂-hBN-WSe₂ heterostructure. The tangerine-based heterostructures have the same kind of patterns as are observed for the molybdenum-based heterostructures. As a representative case in Fig. 7, we present the comparison of the energy contribution to the binding energy of indirect magnetoexcitons for MoSe₂-hBN-MoSe₂ heterostructure obtained by solving the Schrödinger equation with the V_{RK} and V_C potentials. The analysis shows that the V_{RK} potential gives higher contributions to the binding energy than the Coulomb potential for all states, and these contributions increase with the increase of the magnetic field. The same qualitative patterns are observed in other heterostructures.

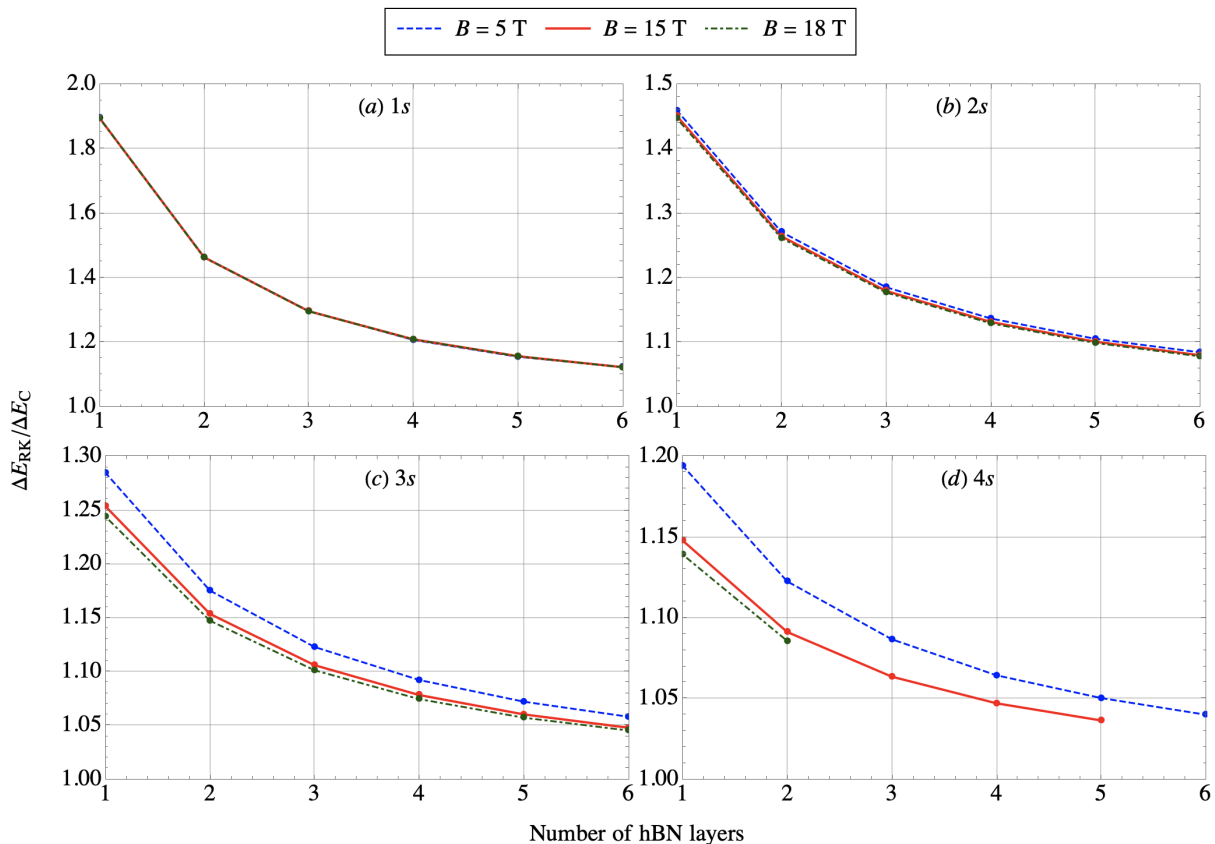


FIG. 4. Ratio of $\Delta E_{RK}/\Delta E_C$ for A_{high} magnetoexcitons in MoS₂-hBN-MoS₂ heterostructure for Rydberg states $1s$ (a), $2s$ (b), $3s$ (c), and $4s$ (d).

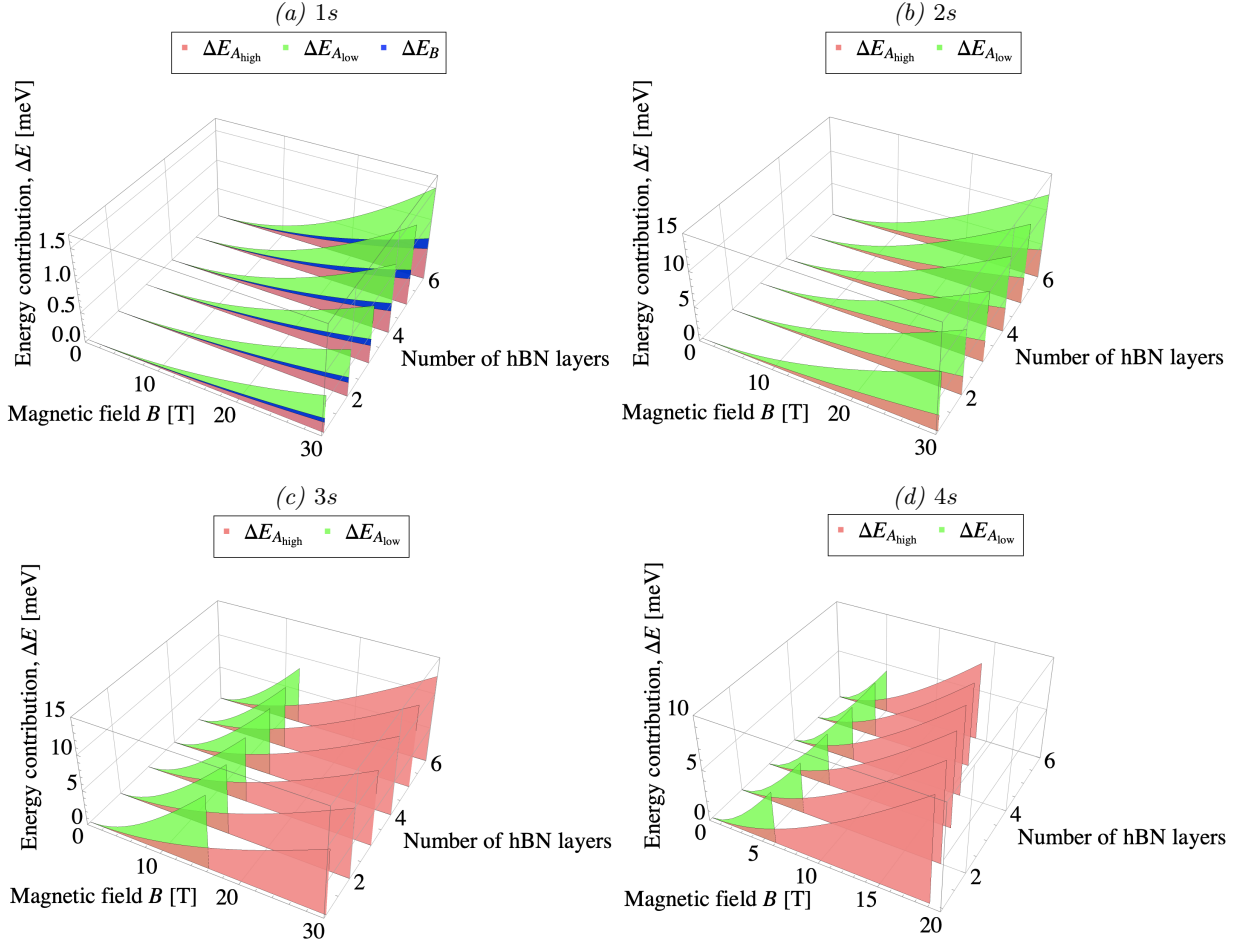


FIG. 5. The energy contribution from the magnetic field to the binding energies of indirect magnetoexcitons in $\text{MoS}_2\text{-hBN-MoS}_2$ heterostructure for Rydberg states $1s$ (a), $2s$ (b), $3s$ (c), and $4s$ (d). Calculations are performed using the Rytova-Keldysh potential.

C. Diamagnetic coefficients

The diamagnetic coefficients $\sigma_{A_{\text{high/low}}}$ for A and σ_B for B direct magnetoexcitons in encapsulated MX_2 monolayers obtained in the framework of our approach are reported in Ref. [74]. Here we report DMCs for direct magnetoexcitons in FS MX_2 monolayers and indirect magnetoexcitons in FS $\text{MX}_2\text{-MX}_2$ bilayers and $\text{MX}_2\text{-hBN-MX}_2$ heterostructures.

The DMCs of direct magnetoexcitons in FS monolayers along with the DMCs for magnetoexcitons in encapsulated WSe_2 , WS_2 , MoSe_2 , and MoS_2 are presented in Table II. Calculations are performed using the V_{RK} potential. The DMCs $\sigma_{A_{\text{high}}} < \sigma_B < \sigma_{A_{\text{low}}}$ for all states. For the $1s$ state $\sigma_{\text{hBN}} > \sigma_{\text{FS}}$ and the ratio $\sigma_{\text{hBN}}/\sigma_{\text{FS}}$ varies from 1.6 to 2.6, depending on monolayer parameters. For the $2s$ state this ratio significantly exceeds 2.6. Therefore, the screening effect in encapsulated monolayers substantially increases the value of DMCs.

Results of calculations of DMCs for molybdenum and tungsten-based heterostructures are presented in Tables IV and V, respectively. We present results for $\sigma_{A_{\text{high}}}$ and $\sigma_{A_{\text{low}}}$ for indirect A magnetoexcitons obtained with parameters for each material that give the highest and lowest binding energies, $E_{A_{\text{high/low}}}$ for A excitons and σ_B for B magnetoexcitons, respectively. For each type of indirect magnetoexciton, we report two sets of σ : one from solution of the Schrödinger equation with V_{RK} potential, another one from solution of the Schrödinger equation using V_C potential. The data analysis of Tables IV and V shows the following important features for both molybdenum and tungsten-based heterostructures: i. the DMCs of the A and B magnetoexcitons increase when the number of hBN layers increase; ii. the DMCs obtained using Rytova-Keldysh potential are always bigger than one obtained for the Coulomb potential; iii. for the states $3s$ and $4s$ $E_0 \sim |E(B) - E_0|$ and Eq. (8) cannot be applied to extract $\sigma_{A_{\text{high/low}}}$ and σ_B from data; iv. for both the RK and Coulomb potentials $\sigma_{A_{\text{high}}} < \sigma_B < \sigma_{A_{\text{low}}}$. The latter indicates that DMCs are sensitive to the exciton reduced mass and polarizability of material: the smaller reduced mass of exciton and larger polarizability lead to the bigger DMC value. A distinct feature of molybdenum-based heterostructures is that for the $2s$ state the DMCs exist in the heterostructure with up to four hBN layers, while in the tungsten-based

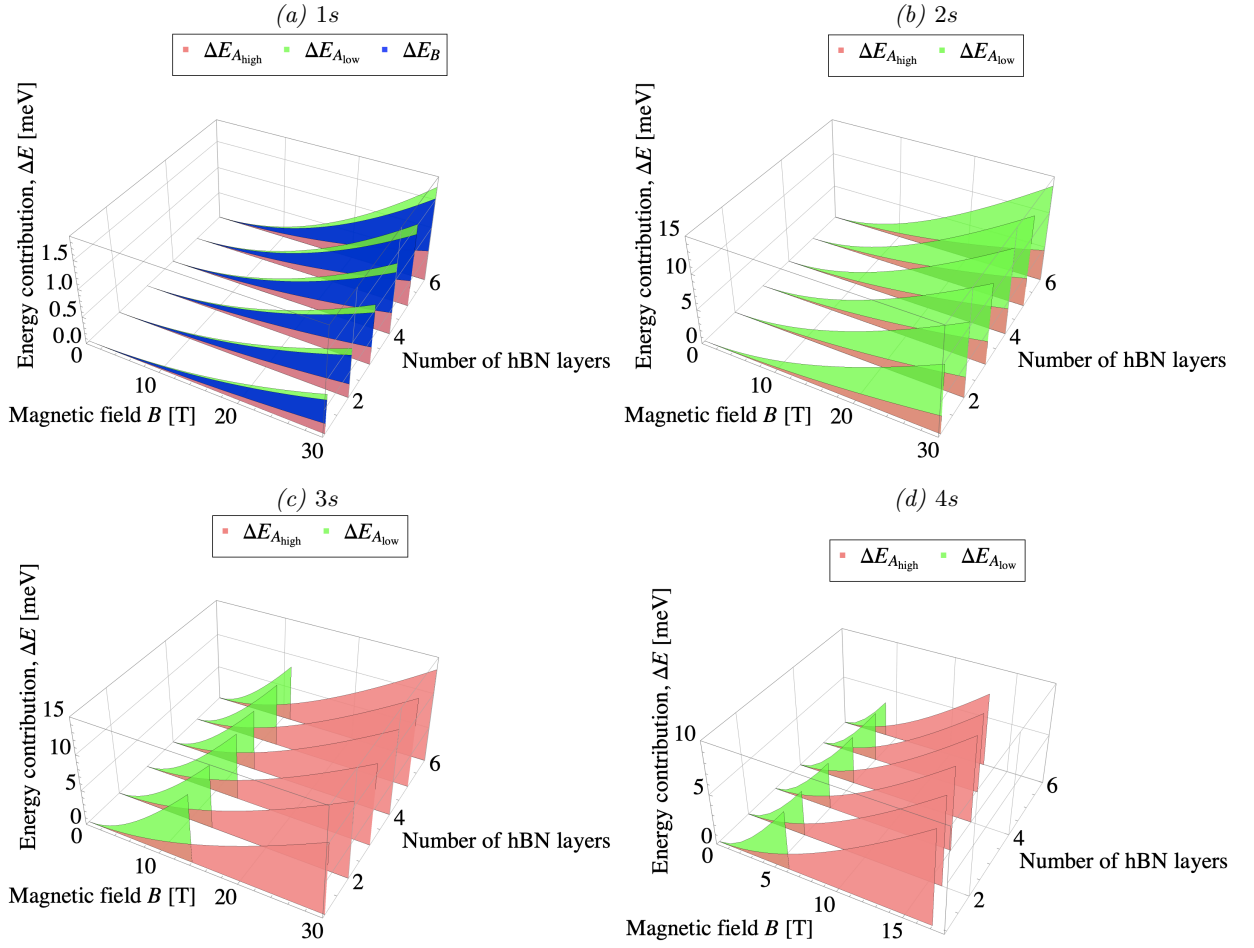


FIG. 6. The energy contribution from the magnetic field to the binding energies of indirect magnetoexcitons in WSe_2 -hBN- WSe_2 heterostructure for Rydberg states $1s$ (a), $2s$ (b), $3s$ (c), and $4s$ (d), respectively. Calculations are performed using the Rytova-Keldysh potential.

TABLE II. The diamagnetic coefficients σ_{FS} of direct magnetoexcitons in FS MX_2 monolayers along with DMCs σ_{hBN} in encapsulated MX_2 monolayers reported in Ref. [74]. DMCs are given in $\mu\text{eV}/\text{T}^2$.

Exciton	1s			2s			3s	
	σ_{FS}	σ_{hBN} [74]	$\sigma_{\text{hBN}}/\sigma_{\text{FS}}$	σ_{FS}	σ_{hBN} [74]	$\sigma_{\text{hBN}}/\sigma_{\text{FS}}$	σ_{FS}	
WSe_2	A_{high}	0.09	0.16	1.78	0.89	2.58	2.90	3.00
	A_{low}	0.34	0.66	1.94	3.34	10.01	3.00	
	B	0.28	0.57	2.04	2.79	8.84	3.17	
WS_2	A_{high}	0.11	0.21	1.91	1.10	3.56	3.24	3.81
	A_{low}	0.29	0.60	2.07	2.94	9.65	3.28	
	B	0.28	0.61	2.18	2.82	9.84	3.45	
MoSe_2	A_{high}	0.08	0.13	1.63	0.74	1.96	2.65	2.44
	A_{low}	0.11	0.18	1.64	1.02	2.76	2.71	
	B	0.09	0.17	1.89	0.85	2.55	3.00	
MoS_2	A_{high}	0.08	0.21	2.63	0.77	3.56	4.62	2.61
	A_{low}	0.28	0.55	1.96	2.77	8.64	3.12	
	B	0.11	0.22	2.00	1.08	3.50	3.24	

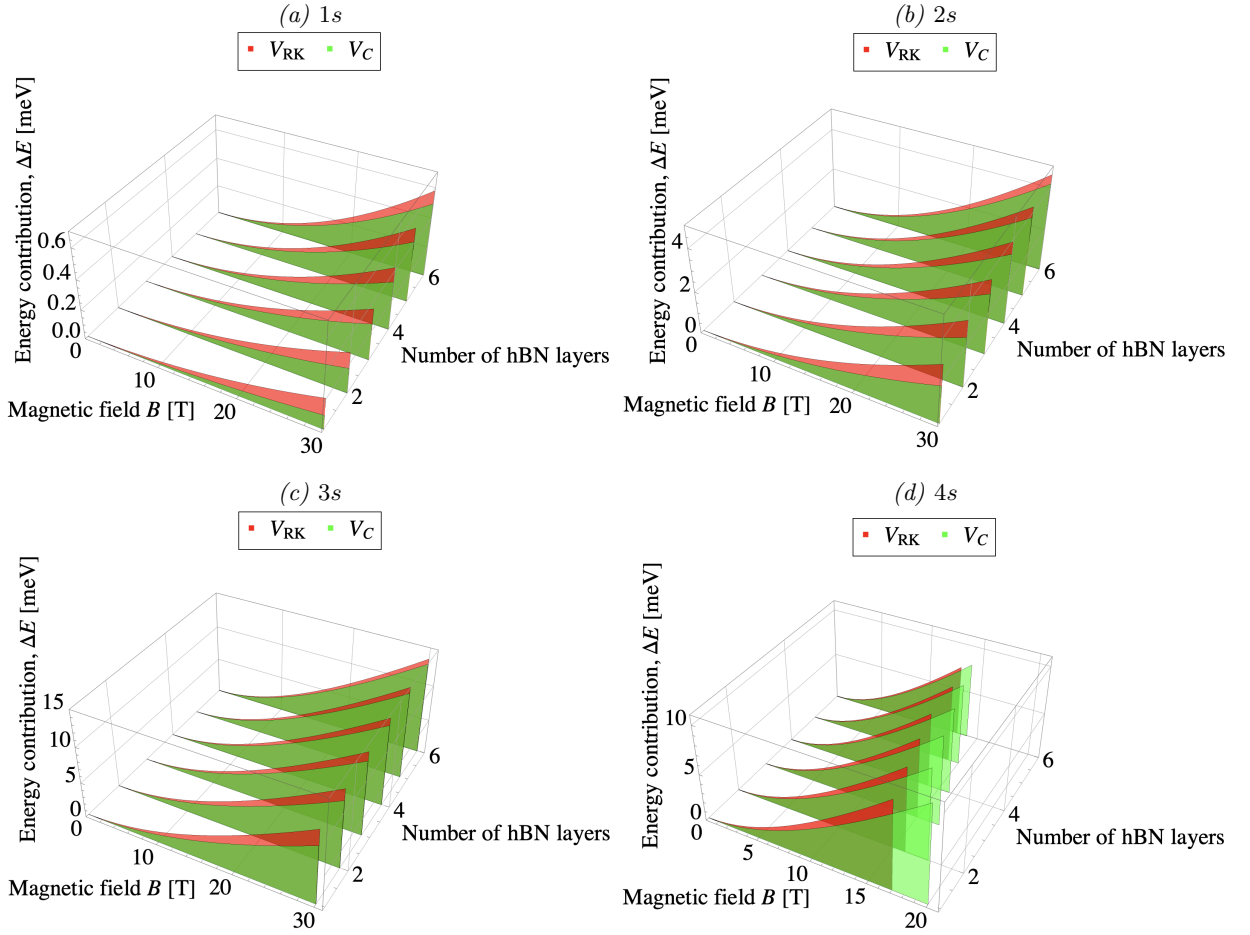


FIG. 7. Comparison between energy contribution when Schrödinger equation is solved with the RK and Coulomb potentials for indirect A_{low} magnetoexcitons in MoSe_2 -hBN- MoSe_2 heterostructure for Rydberg states 1s (a), 2s (b), 3s (c), and 4s (d), respectively.

TABLE III. The diamagnetic coefficients of indirect magnetoexcitons in FS MX_2 - MX_2 bilayers. σ is given in $\mu\text{eV}/\text{T}^2$.

Exciton	1s			2s			3s			4s			
	σ_{RK}	σ_C	σ_{RK}/σ_C	σ_{RK}	σ_C	σ_{RK}/σ_C	σ_{RK}	σ_C	σ_{RK}/σ_C	σ_{RK}	σ_C	σ_{RK}/σ_C	
WSe_2	A_{high}	0.15	0.04	3.75	1.10	0.32	3.44	3.45	1.20	2.88	7.73	3.21	2.41
	A_{low}	0.47	0.12	3.92	3.90	1.21	3.22	12.49	5.06	2.47	27.03		
	B	0.40	0.11	3.64	3.29	1.05	3.13		4.31				
WS_2	A_{high}	0.09	0.05	1.8	0.89	0.43	2.07	3.00	1.69	1.78		4.65	
	A_{low}	0.34	0.11	3.09	3.34	1.15	2.9		4.87				
	B	0.28	0.11	2.55	2.79	1.15	2.43		4.87				
MoSe_2	A_{high}	0.13	0.03	4.33	0.91	0.23	3.95	2.79	0.85	3.28		2.24	
	A_{low}	0.17	0.04	4.25	1.23	0.31	3.97	3.82	1.18	3.24		3.17	
	B	0.14	0.03	4.67	1.05	0.27	3.89	3.22	0.99	3.25		2.65	
MoS_2	A_{high}	0.13	0.03	4.33	0.95	0.28	3.39	3.00	1.05	2.86		2.82	
	A_{low}	0.39	0.10	3.9	3.23	0.99	3.26		4.14				
	B	0.17	0.05	3.4	1.31	0.39	3.36	4.19	1.52	2.76		4.16	

TABLE IV. The diamagnetic coefficients of indirect magnetoexcitons in the molybdenum-based heterostructures. σ is given in $\mu\text{eV}/\text{T}^2$.

State	N	MoSe ₂ -hBN-MoSe ₂						MoS ₂ -hBN-MoS ₂					
		$\sigma_{A_{\text{high}}}$		$\sigma_{A_{\text{low}}}$		σ_B		$\sigma_{A_{\text{high}}}$		$\sigma_{A_{\text{low}}}$		σ_B	
		V_{RK}	V_C	V_{RK}	V_C	V_{RK}	V_C	V_{RK}	V_C	V_{RK}	V_C	V_{RK}	V_C
1s	1	0.17	0.08	0.23	0.11	0.20	0.09	0.19	0.10	0.67	0.37	0.22	0.14
	2	0.23	0.14	0.30	0.19	0.26	0.16	0.25	0.17	0.85	0.58	0.35	0.24
	3	0.29	0.21	0.28	0.27	0.33	0.24	0.33	0.25	1.04	0.81	0.45	0.35
	4	0.35	0.28	0.47	0.36	0.40	0.32	0.41	0.34	1.25	1.04	0.55	0.46
	5	0.42	0.35	0.56	0.46	0.48	0.39	0.49	0.43	1.47	1.27	0.66	0.57
	6	0.50	0.43	0.65	0.55	0.56	0.48	0.58	0.52	1.69	1.51	0.77	0.69
2s	1	2.21	1.41	3.09	2.00		1.67	2.61	1.83			3.75	2.69
	2	2.55	1.90		2.65		2.23	3.03	2.43				
	3	2.90	2.35		3.22		2.74	3.46	2.96				
	4	3.24	2.76										

TABLE V. The diamagnetic coefficients of indirect magnetoexcitons in the tungsten-based heterostructures. σ is given in $\mu\text{eV}/\text{T}^2$.

State	N	WSe ₂ -hBN-WSe ₂						WS ₂ -hBN-WS ₂					
		$\sigma_{A_{\text{high}}}$		$\sigma_{A_{\text{low}}}$		σ_B		$\sigma_{A_{\text{high}}}$		$\sigma_{A_{\text{low}}}$		σ_B	
		V_{RK}	V_C	V_{RK}	V_C	V_{RK}	V_C	V_{RK}	V_C	V_{RK}	V_C	V_{RK}	V_C
1s	1	0.21	0.11	0.80	0.43	0.69	0.37	0.28	0.16	0.74	0.43	0.72	0.37
	2	0.28	0.18	1.00	0.67	0.86	0.58	0.37	0.26	0.94	0.67	0.92	0.58
	3	0.36	0.27	1.21	0.93	1.06	0.81	0.48	0.38	1.16	0.93	1.14	0.81
	4	0.45	0.36	1.44	1.18	1.27	1.04	0.59	0.50	1.39	1.18	1.38	1.04
	5	0.54	0.46	1.68	1.44	1.48	1.27	0.70	0.62	1.63	1.44	1.62	1.27
	6	0.63	0.55	1.93	1.71	1.70	1.51	0.82	0.75	1.88	1.71	1.86	1.51
2s	1	2.92	2.00					4.04	3.00				
	2	3.36	2.65						3.86				

heterostructures, only up to two hBN layers. When the number of hBN layers is more than some specific number, the linear dependence of ΔE on B^2 is invalidated in 2s, 3s, and 4s states for both the Rytova-Keldysh and Coulomb potentials.

IV. CONCLUSION

In the present paper, we have studied energy contributions from the external magnetic field to the binding energies of A and B magnetoexcitons in 1s, 2s, 3s, and 4s Rydberg states in WSe₂, WS₂, MoSe₂, and MoS₂ freestanding and encapsulated monolayers, bilayer MX₂-MX₂, and MX₂-hBN-MX₂ heterostructures. The first time diamagnetic coefficients for the bilayer MX₂-MX₂ and MX₂-hBN-MX₂ heterostructures are calculated and reported. We consider the additional degree of freedom to tailor the binding energies and diamagnetic coefficients for the MX₂-hBN-MX₂ heterostructures by varying the number of hBN sheets between TMDC layers. The study is performed for direct and indirect A and B excitons. For the A magnetoexcitons we used two sets of parameters given in literature that provide the highest (A_{low} exciton) and lowest (A_{high} exciton) binding energy for excitons. For indirect magnetoexcitons in bilayer and van der Waals heterostructures the dependence of energy contribution from the external magnetic field to the binding energies and DMCs are studied using Rytova-Keldysh and Coulomb potentials.

Our study shows that the energy contributions ΔE for direct and indirect magnetoexcitons and DMCs are sensitive to the reduced mass of exciton and the screening distance ρ_0 : the smaller reduced mass and larger ρ_0 lead to the bigger ΔE and DMCs.

The energy contributions ΔE for direct magnetoexcitons increase with the increase of the external magnetic field, and ΔE is more significant for 2s, 3s and 4s states. The DMCs for direct magnetoexcitons in encapsulated monolayers are bigger than in FS monolayers, $\sigma_{\text{hBN}} > \sigma_{\text{FS}}$, and the ratio $\sigma_{\text{hBN}}/\sigma_{\text{FS}}$ varies from 1.6 to 3.6 depending on monolayer parameters and the state of magnetoexcitons. Therefore, the screening effect in encapsulated monolayers significantly increases the value of DMCs.

For our investigation, a two-particle Schrödinger equation for indirect excitons is solved using the Rytova-Keldysh

and Coulomb potentials to calculate binding energies and diamagnetic coefficients. We demonstrate strong sensitivity of the energy contributions from the external magnetic field on the type of the potential: $\Delta E_{RK} > \Delta E_C$ and the difference increases with the increase of the magnetic field. For the B magnetoexcitons for both potentials $\Delta E_{A_{\text{high}}} < \Delta E_B < \Delta E_{A_{\text{low}}}$. The DMCs for $\text{MX}_2\text{-hBN-MX}_2$ heterostructures obtained using Rytova-Keldysh potential are always bigger than one obtained for the Coulomb potential and the DMCs of the A and B magnetoexcitons increase with the increase of the number of hBN layers. However, when the number of hBN layers more than three the difference becomes very small. Such a result is understandable because of the convergence of V_{RK} and V_C potentials with the increase the numbers of hBN layers. Also, a distinct feature of molybdenum-based heterostructures is that DMCs exist for the heterostructure with up to four hBN layers, while tungsten-based heterostructures only up to two hBN layers due to magnetoexcitons dissociation.

In the considered range of the magnetic field, the direct and indirect magnetoexcitons have stable $1s$ and $2s$ Rydberg states. The $3s$ and $4s$ states magnetoexcitons dissociate at some values of the magnetic field depending on parameters of material. The $3s$ and $4s$ states indirect magnetoexcitons bound by the Coulomb potential dissociate at a lower magnetic field than magnetoexcitons bound by the RK potential.

Related to bilayer $\text{MX}_2\text{-MX}_2$: the magnetic field's contribution to the magnetoexcitons binding energies is systematically bigger for the FS bilayer than for the FS MX_2 monolayer for all states when the Rytova-Keldysh potential is used in calculations. The same conclusion is extended to DMCs.

Finally, our results raise the possibility of controlling the binding energies of direct and indirect magnitoexcitons in monolayer MX_2 , bilayer $\text{MX}_2\text{-MX}_2$ and $\text{MX}_2\text{-hBN-MX}_2$ heterostructures using the external magnetic field and open the additional degree of freedom to tailor the binding energies and diamagnetic coefficients for the $\text{MX}_2\text{-hBN-MX}_2$ heterostructures by varying the number of hBN sheets between TMDC layers.

Acknowledgments. This work is supported by the U.S. Department of Defense under Gran No. W911NF1810433 and PSC-CUNY Award No. 62261-00 50.

-
- [1] R. Cheng, D. Li, H. Zhou, C. Wang, A. Yin, S. Jiang, Y. Liu, Y. Chen, Y. Huang, and X. Duan, Electroluminescence and photocurrent generation from atomically sharp $\text{WSe}_2/\text{MoS}_2$ heterojunction p-n diodes, *Nano Lett.* **14**, 5590 (2014).
 - [2] C.-H. Lee, G.-H. Lee, A. Zande, W. Chen, Y. Li, M. Han, X. Cui, G. Arefe, C. Nuckolls, T. Heinz, J. Guo, J. Hone, and P. Kim, Atomically thin p-n junctions with van der Waals heterointerfaces, *Nat. Nanotechnol.* **9**, 676–681 (2014).
 - [3] B. Peng, P. K. Ang, and K. P. Loh, Two-dimensional dichalcogenides for light-harvesting applications, *Nano Today* **10**, 128 (2015).
 - [4] K. S. Novoselov, A. Mishchenko, A. Carvalho, and A. H. Castro Neto, 2D materials and van der Waals heterostructures, *Science* **353** (2016).
 - [5] D. Marian, E. Dib, T. Cusati, E. G. Marin, A. Fortunelli, G. Iannaccone, and G. Fiori, Transistor concepts based on lateral heterostructures of metallic and semiconducting phases of MoS_2 , *Phys. Rev. Applied* **8**, 054047 (2017).
 - [6] C. Li, P. Zhou, and D. Zhang, Devices and applications of van der Waals heterostructures, *J. Semicond* **38**, 031005 (2017).
 - [7] G. Iannaccone, F. Bonaccorso, L. Colombo, and G. Fiori, Quantum engineering of transistors based on 2D materials heterostructures, *Nat. Nanotechnol.* **13** (2018).
 - [8] H. Xue, Y. Wang, Y. Dai, W. Kim, H. Jussila, M. Qi, J. Susoma, Z. Ren, Q. Dai, J. Zhao, K. Halonen, H. Lipsanen, X. Wang, X. Gan, and Z. Sun, A $\text{MoSe}_2/\text{WSe}_2$ heterojunction-based photodetector at telecommunication wavelengths, *Adv. Funct. Mater.* **28**, 1804388 (2018).
 - [9] C. Tang, Y. Min, C. Chen, W. Xu, and L. Xu, Potential applications of heterostructures of TMDs with MXenes in sodium-Ion and Na-O2 batteries, *Nano Lett.* **19** (2019).
 - [10] G. Migliato Marega, Y. Zhao, A. Avsar, Z. Wang, M. Tripathi, A. Radenovic, and A. Kis, Logic-in-memory based on an atomically thin semiconductor, *Nature* **587**, 72 (2020).
 - [11] K. F. Mak, C. Lee, J. Hone, J. Shan, and T. F. Heinz, Atomically thin MoS_2 : A new direct-gap semiconductor, *Phys. Rev. Lett.* **105**, 136805 (2010).
 - [12] A. Splendiani, L. Sun, Y. Zhang, T. Li, J. Kim, C.-Y. Chim, G. Galli, and F. Wang, Emerging photoluminescence in monolayer MoS_2 , *Nano Lett.* **10**, 1271 (2010).
 - [13] S. Tongay, J. Zhou, C. Ataca, K. Lo, T. S. Matthews, J. Li, J. C. Grossman, and J. Wu, Thermally driven crossover from indirect toward direct bandgap in 2D semiconductors: MoSe_2 versus MoS_2 , *Nano Lett.* **12**, 5576 (2012).
 - [14] G. Wang, A. Chernikov, M. M. Glazov, T. F. Heinz, X. Marie, T. Amand, and B. Urbaszek, Colloquium: Excitons in atomically thin transition metal dichalcogenides, *Rev. Mod. Phys.* **90**, 021001 (2018).
 - [15] K. Kořmider, J. W. González, and J. Fernández-Rossier, Large spin splitting in the conduction band of transition metal dichalcogenide monolayers, *Phys. Rev. B* **88**, 245436 (2013).
 - [16] H. Zeng, G.-B. Liu, J. Dai, Y. Yan, B. Zhu, R. He, L. Xie, S. Xu, X. Chen, W. Yao, and X. Cui, Optical signature of symmetry variations and spin-valley coupling in atomically thin tungsten dichalcogenides, *Sci. Rep.* **3**, 1608 (2013).
 - [17] M. Fogler, L. Butov, and K. Novoselov, High-temperature superfluidity with indirect excitons in van der Waals het-

- erostuctures, *Nat. Commun.* **5**, 4555 (2014).
- [18] O. L. Berman and R. Ya. Kezerashvili, High-temperature superfluidity of the two-component Bose gas in a transition metal dichalcogenide bilayer, *Phys. Rev. B* **93**, 245410 (2016).
- [19] E. Calman, M. Fogler, L. Butov, S. Hu, A. Mishchenko, and A. Geim, Indirect excitons in van der Waals heterostructures at room temperature, *Nat. Commun.* **9** (2018).
- [20] E. V. Calman, L. H. Fowler-Gerace, D. J. Choksy, L. V. Butov, D. E. Nikonov, I. A. Young, S. Hu, A. Mishchenko, and A. K. Geim, Indirect excitons and trions in MoSe₂/WSe₂ van der Waals heterostructures, *Nano Lett.* **20**, 1869 (2020).
- [21] O. L. Berman, R. Ya. Kezerashvili, Y. E. Lozovik, and K. G. Ziegler, Electron-hole superfluidity controlled by a periodic potential, *Phys. Rev. B* **100**, 134514 (2019).
- [22] M. Van der Donck, S. Conti, A. Perali, A. R. Hamilton, B. Partoens, F. M. Peeters, and D. Neilson, Three-dimensional electron-hole superfluidity in a superlattice close to room temperature, *Phys. Rev. B* **102**, 060503 (2020).
- [23] O. L. Berman and R. Ya. Kezerashvili, Superfluidity of dipolar excitons in a transition metal dichalcogenide double layer, *Phys. Rev. B* **96**, 094502 (2017).
- [24] O. Cotlet, S. Zeytinoglu, M. Sigrist, E. Demler, and A. Imamoğlu, Superconductivity and other collective phenomena in a hybrid Bose-Fermi mixture formed by a polariton condensate and an electron system in two dimensions, *Phys. Rev. B* **93**, 054510 (2016).
- [25] S. Manzeli, D. Ovchinnikov, D. Pasquier, O. V. Yazyev, and A. Kis, 2D transition metal dichalcogenides, *Nat. Rev. Mater.* **2**, 17033 (2017).
- [26] R. Ya. Kezerashvili, Few-body systems in condensed matter physics, *Few-Body Syst.* **60**, 52 (2019).
- [27] D. Wickramaratne, F. Zahid, and R. K. Lake, Electronic and thermoelectric properties of few-layer transition metal dichalcogenides, *J. Chem. Phys.* **140**, 124710 (2014).
- [28] P. Rivera, J. Schaibley, A. Jones, J. Ross, S. Wu, G. Aivazian, P. Klement, N. Ghimire, J.-Q. Yan, D. Mandrus, W. Yao, and X. Xu, Observation of long-lived interlayer excitons in monolayer MoSe₂-WSe₂ heterostructures, *Nat. Commun.* **6** (2014).
- [29] M. Palummo, M. Bernardi, and J. C. Grossman, Exciton radiative lifetimes in two-dimensional transition metal dichalcogenides, *Nano Lett.* **15**, 2794 (2015).
- [30] H. Chen, X. Wen, J. Zhang, T. Wu, Y. Gong, X. Zhang, J. Yuan, C. Yi, J. Lou, P. Ajayan, W. Zhuang, G. Zhang, and J. Zheng, Ultrafast formation of interlayer hot excitons in atomically thin MoS₂/WS₂ heterostructures, *Nat. Commun.* **7**, 12512 (2016).
- [31] P. Nagler, G. Plechinger, M. Ballottin, M. Anatolie, S. Meier, N. Paradiso, C. Strunk, A. Chernikov, P. Christianen, C. Schüller, and T. Korn, Interlayer exciton dynamics in a dichalcogenide monolayer heterostructure, *2D Mater.* **4** (2017).
- [32] Q. Li, L. Tang, C. Zhang, D. Wang, Q.-J. Chen, Y.-X. Feng, L.-M. Tang, and K.-Q. Chen, Seeking the Dirac cones in the MoS₂/WSe₂ van der Waals heterostructure, *Appl. Phys. Lett.* **111**, 171602 (2017).
- [33] P. Rivera, K. L. Seyler, H. Yu, J. R. Schaibley, J. Yan, D. G. Mandrus, W. Yao, and X. Xu, Valley-polarized exciton dynamics in a 2D semiconductor heterostructure, *Science* **351**, 688 (2016).
- [34] P. Rivera, H. Yu, K. Seyler, N. Wilson, W. Yao, and X. Xu, Interlayer valley excitons in heterobilayers of transition metal dichalcogenides, *Nat. Nanotechnol.* **13** (2018).
- [35] M. Van der Donck and F. M. Peeters, Interlayer excitons in transition metal dichalcogenide heterostructures, *Phys. Rev. B* **98**, 115104 (2018).
- [36] J. Kunstmann, F. Mooshammer, P. Nagler, A. Chaves, F. Stein, N. Paradiso, G. Plechinger, C. Strunk, C. Schüller, G. Seifert, D. Reichman, and T. Korn, Momentum-space indirect interlayer excitons in transition metal dichalcogenide van der Waals heterostructures, *Nat. Phys.* **14** (2018).
- [37] S. Ovesen, S. Brem, C. Linderälv, M. Kuisma, T. Korn, P. Erhart, M. Selig, and E. Malic, Interlayer exciton dynamics in van der Waals heterostructures, *Commun. Phys.* **2**, 23 (2019).
- [38] E. V. Calman, C. J. Dorow, M. M. Fogler, L. V. Butov, S. Hu, A. Mishchenko, and A. K. Geim, Control of excitons in multi-layer van der Waals heterostructures, *Appl. Phys. Lett.* **108**, 101901 (2016).
- [39] J. He, K. Hummer, and C. Franchini, Stacking effects on the electronic and optical properties of bilayer transition metal dichalcogenides MoS₂, MoSe₂, WS₂, and WSe₂, *Phys. Rev. B* **89**, 075409 (2014).
- [40] X. Hu, L. Kou, and L. Sun, Stacking orders induced direct band gap in bilayer MoSe₂-WSe₂ lateral heterostructures, *Sci. Rep.* **6**, 31122 (2016).
- [41] Y. Zhang, T.-R. Chang, B. Zhou, Y.-T. Cui, H. Yan, Z. Liu, F. Schmitt, J. Lee, R. Moore, Y. Chen, H. Lin, H.-T. Jeng, S.-K. Mo, Z. Hussain, A. Bansil, and Z.-X. Shen, Direct observation of the transition from indirect to direct bandgap in atomically thin epitaxial MoSe₂, *Nat. Nanotechnol.* **9** (2013).
- [42] L. Debbichi, O. Eriksson, and S. Lebegue, Electronic structure of two-dimensional transition metal dichalcogenide bilayers from ab initio theory, *Phys. Rev. B* **89**, 205311 (2014).
- [43] B. Amin, N. Singh, and U. Schwingenschlögl, Heterostructures of transition metal dichalcogenides, *Phys. Rev. B* **92**, 075439 (2015).
- [44] H. Terrones, F. López-Urías, and M. Terrones, Novel hetero-layered materials with tunable direct band gaps by sandwiching different metal disulfides and diselenides, *Sci. Rep.* **3**, 1549 (2013).
- [45] L. A. Jauregui, A. Y. Joe, K. Pistunova, D. S. Wild, A. A. High, Y. Zhou, G. Scuri, K. De Greve, A. Sushko, C.-H. Yu, T. Taniguchi, K. Watanabe, D. J. Needleman, M. D. Lukin, H. Park, and P. Kim, Electrical control of interlayer exciton dynamics in atomically thin heterostructures, *Science* **366**, 870 (2019).
- [46] H. Kamban and T. Pedersen, Interlayer excitons in van der Waals heterostructures: Binding energy, Stark shift, and field-induced dissociation, *Sci. Rep.* **10** (2020).

- [47] B. Miller, A. Steinhoff, B. Pano, J. Klein, F. Jahnke, A. Holleitner, and U. Wurstbauer, Long-lived direct and indirect interlayer excitons in van der Waals heterostructures, *Nano Lett.* **17**, 5229 (2017).
- [48] R. Elliott and R. Loudon, Theory of the absorption edge in semiconductors in a high magnetic field, *J. Phys. Chem. Solids* **15**, 196 (1960).
- [49] H. Hasegawa and R. Howard, Optical absorption spectrum of hydrogenic atoms in a strong magnetic field, *J. Phys. Chem. Solids* **21**, 179 (1961).
- [50] M. Shinada and S. Sugano, Optical absorption edge in layer-type semiconductors, *J. Phys. Soc. Jpn.* **20**, 1274 (1965).
- [51] L. P. GorKov and I. E. Dzuloshinskii, Contribution to the theory of the Mott exciton in a strong magnetic field, *Zh. Eksp. Teor. Fiz.* **53**, 717 (1967).
- [52] O. Akimoto and H. Hasegawa, Interband optical transitions in extremely anisotropic semiconductors. II. Coexistence of exciton and the Landau levels, *J. Phys. Soc. Jpn.* **22**, 181 (1967).
- [53] I. Kylänpää and H.-P. Komsa, Binding energies of exciton complexes in transition metal dichalcogenide monolayers and effect of dielectric environment, *Phys. Rev. B* **92**, 205418 (2015).
- [54] A. Stier, K. McCreary, B. Jonker, J. Kono, and S. Crooker, Exciton diamagnetic shifts and valley Zeeman effects in monolayer WS₂ and MoS₂ to 65 Tesla, *Nat. Commun.* **7**, 10643 (2016).
- [55] J. Zipfel, J. Holler, A. A. Mitioglu, M. V. Ballottin, P. Nagler, A. V. Stier, T. Taniguchi, K. Watanabe, S. A. Crooker, P. C. M. Christianen, T. Korn, and A. Chernikov, Spatial extent of the excited exciton states in WS₂ monolayers from diamagnetic shifts, *Phys. Rev. B* **98**, 075438 (2018).
- [56] A. V. Stier, N. P. Wilson, K. A. Velizhanin, J. Kono, X. Xu, and S. A. Crooker, Magneto-optics of exciton Rydberg states in a monolayer semiconductor, *Phys. Rev. Lett.* **120**, 057405 (2018).
- [57] E. Liu, J. van Baren, T. Taniguchi, K. Watanabe, Y.-C. Chang, and C. H. Lui, Magnetophotoluminescence of exciton Rydberg states in monolayer WS₂, *Phys. Rev. B* **99**, 205420 (2019).
- [58] M. Goryca, J. Li, A. Stier, T. Taniguchi, K. Watanabe, E. Courtade, S. Shree, C. Robert, B. Urbaszek, X. Marie, and S. Crooker, Revealing exciton masses and dielectric properties of monolayer semiconductors with high magnetic fields, *Nat. Commun.* **10** (2019).
- [59] T. Goldstein, Y.-C. Wu, S.-Y. Chen, T. Taniguchi, K. Watanabe, K. Varga, and J. Yan, Ground and excited state exciton polarons in monolayer MoSe₂, *J. Chem. Phys.* **153**, 071101 (2020).
- [60] G. Aivazian, Z. Gong, A. Jones, R.-L. Chu, J.-Q. Yan, D. Mandrus, C. Zhang, D. Cobden, W. Yao, and X. Xu, Magnetic control of valley pseudospin in monolayer WSe₂, *Nat. Phys.* **11** (2014).
- [61] A. Srivastava, M. Sidler, A. Allain, D. Lembke, A. Kis, and A. Imamoglu, Valley Zeeman effect in elementary optical excitations of a monolayer WSe₂, *Nat. Phys.* **11** (2014).
- [62] Y. Li, J. Ludwig, T. Low, A. Chernikov, X. Cui, G. Arefe, Y. D. Kim, A. M. van der Zande, A. Rigosi, H. M. Hill, S. H. Kim, J. Hone, Z. Li, D. Smirnov, and T. F. Heinz, Valley splitting and polarization by the Zeeman effect in monolayer MoSe₂, *Phys. Rev. Lett.* **113**, 266804 (2014).
- [63] D. MacNeill, C. Heikes, K. Mak, Z. Anderson, A. Kormányos, V. Zólyomi, J. Park, and D. Ralph, Breaking of valley degeneracy by magnetic field in monolayer MoSe₂, *Phys. Rev. Lett.* **114** (2014).
- [64] G. Plechinger, P. Nagler, A. Arora, A. Aguila, M. Ballottin, T. Frank, P. Steinleitner, M. Gmitra, J. Fabian, P. Christianen, R. Bratschitsch, C. Schüller, and T. Korn, Excitonic valley effects in monolayer WS₂ under high magnetic fields, *Nano Lett.* **16** (2016).
- [65] D. V. Rybkovskiy, I. C. Gerber, and M. V. Durnev, Atomically inspired $k \cdot p$ approach and valley Zeeman effect in transition metal dichalcogenide monolayers, *Phys. Rev. B* **95**, 155406 (2017).
- [66] M. Van der Donck, M. Zarenia, and F. M. Peeters, Strong valley Zeeman effect of dark excitons in monolayer transition metal dichalcogenides in a tilted magnetic field, *Phys. Rev. B* **97**, 081109 (2018).
- [67] M. Koperski, M. Molas, A. Arora, K. Nogajewski, M. Bartos, J. Wyzula, D. Vaclavkova, P. Kossacki, and M. Potemski, Orbital, spin and valley contributions to Zeeman splitting of excitonic resonances in MoSe₂, WSe₂ and WS₂ monolayers, *2D Mater.* **6**, 015001 (2018).
- [68] S.-Y. Chen, Z. Lu, T. Goldstein, J. Tong, A. Chaves, J. Kunstmann, L. S. R. Cavalcante, T. Woźniak, G. Seifert, D. R. Reichman, T. Taniguchi, K. Watanabe, D. Smirnov, and J. Yan, Luminescent emission of excited Rydberg excitons from monolayer WSe₂, *Nano Lett.* **19**, 2464 (2019).
- [69] F. Xuan and S. Y. Quek, Valley Zeeman effect and Landau levels in two-dimensional transition metal dichalcogenides, *Phys. Rev. Research* **2**, 033256 (2020).
- [70] F. Luckert, M. Yakushev, C. Faugeras, A. Karotki, A. Mudryi, and R. Martin, Diamagnetic shift of the A free exciton in CuGaSe₂ single crystals, *Appl. Phys. Lett.* **97**, 162101 (2010).
- [71] B. Choi, Y. Kim, and J. Song, Diamagnetic shift of a InGaP-AlInGaP semiconductor single quantum well under pulsed-magnetic fields, *Applied Science and Convergence Technology* **24**, 156 (2015).
- [72] M. Van der Donck, M. Zarenia, and F. M. Peeters, Excitons, trions, and biexcitons in transition-metal dichalcogenides: Magnetic-field dependence, *Phys. Rev. B* **97**, 195408 (2018).
- [73] B. Han, C. Robert, E. Courtade, M. Manca, S. Shree, T. Amand, P. Renucci, T. Taniguchi, K. Watanabe, X. Marie, L. E. Golub, M. M. Glazov, and B. Urbaszek, Exciton states in monolayer MoSe₂ and MoTe₂ probed by upconversion spectroscopy, *Phys. Rev. X* **8**, 031073 (2018).
- [74] A. Spiridonova, Magnetoexcitons in monolayer transition-metal dichalcogenides, *Phys. Lett. A* **384**, 126850 (2020).
- [75] F. Cadiz, E. Courtade, C. Robert, G. Wang, Y. Shen, H. Cai, T. Taniguchi, K. Watanabe, H. Carrere, D. Lagarde, M. Manca, T. Amand, P. Renucci, S. Tongay, X. Marie, and B. Urbaszek, Excitonic linewidth approaching the homogeneous limit in MoS₂-based van der Waals heterostructures, *Phys. Rev. X* **7**, 021026 (2017).

- [76] I. C. Gerber and X. Marie, Dependence of band structure and exciton properties of encapsulated WSe₂ monolayers on the hBN-layer thickness, *Phys. Rev. B* **98**, 245126 (2018).
- [77] M. N. Brunetti, O. L. Berman, and R. Ya. Kezerashvili, Optical absorption by indirect excitons in a transition metal dichalcogenide/hexagonal boron nitride heterostructure, *J. Phys.: Condens. Matter* **30**, 225001 (2018).
- [78] J. Lindlau, M. Selig, A. Neumann, L. Colombier, J. Förste, V. Funk, M. Förg, J. Kim, G. Berghäuser, T. Taniguchi, K. Watanabe, F. Wang, E. Malic, and A. Högele, The role of momentum-dark excitons in the elementary optical response of bilayer WSe₂, *Nat. Commun.* **9** (2018).
- [79] A. Arora, M. Koperski, A. Slobodeniuk, K. Nogajewski, R. Schmidt, R. Schneider, M. R. Molas, S. M. de Vasconcellos, R. Bratschitsch, and M. Potemski, Zeeman spectroscopy of excitons and hybridization of electronic states in few-layer WSe₂, MoSe₂ and MoTe₂, *2D Mater.* **6**, 015010 (2018).
- [80] K. L. Seyler, P. Rivera, H. Yu, N. P. Wilson, E. L. Ray, D. G. Mandrus, J. Yan, W. Yao, and X. Xu, Signatures of moiré-trapped valley excitons in MoSe₂/WSe₂ heterobilayers, *Nature* **567**, 66 (2019).
- [81] T. Wang, S. Miao, Z. Li, Y. Meng, Z. Lu, Z. Lian, M. Blei, T. Taniguchi, K. Watanabe, S. Tongay, D. Smirnov, and S.-F. Shi, Giant valley-Zeeman splitting from spin-singlet and spin-triplet interlayer excitons in WSe₂/MoSe₂ heterostructure, *Nano Lett.* **20**, 694 (2020).
- [82] T. Woźniak, P. E. Faria Junior, G. Seifert, A. Chaves, and J. Kunstmann, Exciton *g* factors of van der Waals heterostructures from first-principles calculations, *Phys. Rev. B* **101**, 235408 (2020).
- [83] M. Shinada and K. Tanaka, Interband optical transitions in extremely anisotropic semiconductors. III. Numerical studies of magneto-optical absorption, *J. Phys. Soc. Jpn.* **29**, 1258 (1970).
- [84] I. Lerner and Y. Lozovik, Mott exciton in a quasi-two-dimensional semiconductor in a strong magnetic field, *Zh. Eksp. Teor. Fiz.* **78**, 1167 (1978).
- [85] H. Herold, H. Ruder, and G. Wunner, The two-body problem in the presence of a homogeneous magnetic field, *J. Phys. B: Atom. Mol. Phys.* **14**, 751 (1981).
- [86] A. H. MacDonald and D. S. Ritchie, Hydrogenic energy levels in two dimensions at arbitrary magnetic fields, *Phys. Rev. B* **33**, 8336 (1986).
- [87] C. Stafford, S. Schmitt-Rink, and W. Schaefer, Nonlinear optical response of two-dimensional magnetoexcitons, *Phys. Rev. B* **41**, 10000 (1990).
- [88] Y. Lozovik and A. Ruvinsky, Magnetoexcitons in coupled quantum wells, *Phys. Lett. A* **227**, 271 (1997).
- [89] N. Rytova, Screened potential of a point charge in a thin film, *Proc. Moscow State University, Phys. Astron.* **3**, 30 (1967).
- [90] L. V. Keldysh, Coulomb interaction in thin semiconductor and semimetal films, *JETP Lett* **29**, 658 (1979).
- [91] C. Robert, M. A. Semina, F. Cadiz, M. Manca, E. Courtade, T. Taniguchi, K. Watanabe, H. Cai, S. Tongay, B. Lassagne, P. Renucci, T. Amand, X. Marie, M. M. Glazov, and B. Urbaszek, Optical spectroscopy of excited exciton states in MoSe₂ monolayers in van der Waals heterostructures, *Phys. Rev. Materials* **2**, 011001 (2018).
- [92] A. Chernikov, T. C. Berkelbach, H. M. Hill, A. Rigosi, Y. Li, O. B. Aslan, D. R. Reichman, M. S. Hybertsen, and T. F. Heinz, Exciton binding energy and nonhydrogenic Rydberg series in monolayer WS₂, *Phys. Rev. Lett.* **113**, 076802 (2014).
- [93] M. Z. Mayers, T. C. Berkelbach, M. S. Hybertsen, and D. R. Reichman, Binding energies and spatial structures of small carrier complexes in monolayer transition-metal dichalcogenides via diffusion Monte Carlo, *Phys. Rev. B* **92**, 161404 (2015).
- [94] D. W. Kidd, D. K. Zhang, and K. Varga, Binding energies and structures of two-dimensional excitonic complexes in transition metal dichalcogenides, *Phys. Rev. B* **93**, 125423 (2016).
- [95] D. C. Rogers, J. Singleton, R. J. Nicholas, C. T. Foxon, and K. Woodbridge, Magneto-optics in GaAs-Ga_{1-x}Al_xAs quantum wells, *Phys. Rev. B* **34**, 4002 (1986).
- [96] K. J. Nash, M. S. Skolnick, P. A. Claxton, and J. S. Roberts, Diamagnetism as a probe of exciton localization in quantum wells, *Phys. Rev. B* **39**, 10943 (1989).
- [97] S. N. Walck and T. L. Reinecke, Exciton diamagnetic shift in semiconductor nanostructures, *Phys. Rev. B* **57**, 9088 (1998).
- [98] M. Erdmann, C. Ropers, M. Wenderoth, R. G. Ulbrich, S. Malzer, and G. H. Döhler, Diamagnetic shift of disorder-localized excitons in narrow GaAs/AlGaAs quantum wells, *Phys. Rev. B* **74**, 125412 (2006).
- [99] M. P. F. de Godoy, P. F. Gomes, M. K. K. Nakaema, F. Iikawa, M. J. S. P. Brasil, R. A. Caetano, J. R. Madureira, J. R. R. Bortoleto, M. A. Cotta, E. Ribeiro, G. E. Marques, and A. C. R. Bittencourt, Exciton *g* factor of type-II InP/GaAs single quantum dots, *Phys. Rev. B* **73**, 033309 (2006).
- [100] D. Kim, W. Sheng, P. J. Poole, D. Dalacu, J. Lefebvre, J. Lapointe, M. E. Reimer, G. C. Aers, and R. L. Williams, Tuning the exciton *g* factor in single InAs/InP quantum dots, *Phys. Rev. B* **79**, 045310 (2009).
- [101] M. Abbarchi, T. Kuroda, T. Mano, K. Sakoda, and M. Gurioli, Magneto-optical properties of excitonic complexes in GaAs self-assembled quantum dots, *Phys. Rev. B* **81**, 035334 (2010).
- [102] J. van Bree, A. Y. Silov, P. M. Koenraad, M. E. Flatté, and C. E. Pryor, *g* factors and diamagnetic coefficients of electrons, holes, and excitons in InAs/InP quantum dots, *Phys. Rev. B* **85**, 165323 (2012).
- [103] S. Brodbeck, S. De Liberato, M. Amthor, M. Klaas, M. Kamp, L. Worschech, C. Schneider, and S. Höfling, Experimental verification of the very strong coupling regime in a GaAs quantum well microcavity, *Phys. Rev. Lett.* **119**, 027401 (2017).
- [104] T. C. Berkelbach, M. S. Hybertsen, and D. R. Reichman, Theory of neutral and charged excitons in monolayer transition metal dichalcogenides, *Phys. Rev. B* **88**, 045318 (2013).
- [105] D. Van Tuan, M. Yang, and H. Dery, Coulomb interaction in monolayer transition-metal dichalcogenides, *Phys. Rev. B* **98**, 125308 (2018).
- [106] O. L. Berman, G. Gumbs, and R. Ya. Kezerashvili, Bose-einstein condensation and superfluidity of dipolar excitons in a

- phosphorene double layer, *Phys. Rev. B* **96**, 014505 (2017).
- [107] M. N. Brunetti, O. L. Berman, and R. Ya. Kezerashvili, Optical properties of excitons in buckled two-dimensional materials in an external electric field, *Phys. Rev. B* **98**, 125406 (2018).
 - [108] R. Ya. Kezerashvili and A. Spiridonova, Effects of parallel electric and magnetic fields on Rydberg excitons in buckled two-dimensional materials (2020), arXiv:2011.03093 [cond-mat.mes-hall].
 - [109] M. Florian, M. Hartmann, A. Steinhoff, J. Klein, A. W. Holleitner, J. J. Finley, T. O. Wehling, M. Kaniber, and C. Gies, The dielectric impact of layer distances on exciton and trion binding energies in van der Waals heterostructures, *Nano Lett.* **18**, 2725 (2018).
 - [110] A. Ramasubramaniam, Large excitonic effects in monolayers of molybdenum and tungsten dichalcogenides, *Phys. Rev. B* **86**, 115409 (2012).
 - [111] A. Kormányos, G. Burkard, M. Gmitra, J. Fabian, V. Zólyomi, N. D. Drummond, and V. Fal'ko, k-p theory for two-dimensional transition metal dichalcogenide semiconductors, *2D Mater.* **2**, 022001 (2015).